# **Quantitative Analysis of Magnetic Gradients Performance Changes and Image Quality Following the Application of Sound Reduction Technique in MRI**

# Ho-Beom Lee<sup>1</sup> and Yong-Soo Han<sup>2</sup>\*

<sup>1</sup>Department of Radiology, Wonkwang Health Science University, 514, Iksan-daero, Iksan-si, Republic of Korea <sup>2</sup>Department of Radiological Science, Hanlym Polytechnic University, Chuncheon 24210, Republic of Korea

(Received 8 April 2025, Received in final form 2 July 2025, Accepted 8 July 2025)

This study aimed to quantitatively compare and analyze the changes in sound pressure levels and the differences in image quality before and after applying the Sound reduction technique. We propose the utility of sound reduction techniques and suggest clinically meaningful criteria based on our findings. ACR phantom images, including T1-weight, T2-weight, DWI, and 3D GE T1 sequences, were acquired using a 3.0 T MRI both before and after the application of the Sound reduction technique. We assessed whether the images met quality control guidelines and compared the reductions in sound pressure levels using the displayed SPL values from the equipment. The DWI image was significantly distorted precluding accurate measurement for meeting the ACR MRI phantom guidelines. However, most of the other images showed no significant differences. Although there were statistically significant differences (p < 0.05) in some categories, these images still passed the criteria set by the ACR phantom guidelines. Sound pressure levels were reduced by 27.3%, 49.6%, 72.5%, and 70.1% in the T1, T2, DWI, and 3D GE sequences, respectively. In conclusion, all images except DWI maintained comparable image quality.

Keywords: gradients, sound reduction, sound pressure level

## 1. Introduction

Magnetic Resonance Imaging (MRI) relies on generating magnetic fields through electromagnetic induction, which is caused by the variations in current within the gradient coils. These current changes can lead to vibrations and movements in the gradient coils, creating sound because of interactions with the primary magnetic field [1]. The sound generated is directly related to the Lorentz force exerted on the gradient coils, which is affected by the strength of the primary magnetic field and the amplitude of the gradient coil currents [2]. Consequently, higher magnetic field strengths result in increased sound levels. For example, in 3.0 T MRI systems, the maximum sound pressure level (SPL) can reach up to 125.7 dB(A)during Magnetic Resonance Angiography (MRA) and 130.7 dB(A) during Echo Planar Imaging (EPI), surpassing the 99 dB(A) limit set by the International Electrotechnical Commission (IEC) [3]. This persistent sound not only causes discomfort for patients but can also induce psychological stress, potentially compromising the accuracy of the imaging results. In functional MRI (fMRI), sound can interfere with brain function and alter blood oxygen level-dependent (BOLD) signals, potentially affecting studies focused on auditory pathways and language processing, as it may trigger activation in brain regions associated with auditory processing [4]. Furthermore, excessive sound exposure poses a significant risk of hearing loss. According to the Occupational Safety and Health Administration (OSHA), the permissible sound exposure limit is set at 90 dB(A) for an 8-hour period, with the threshold increasing by 5 dB(A) for every halving of exposure time. For an MRI scan lasting one hour, the allowable exposure limit rises to 105 dB(A). However, the sound levels produced by 3.0 T MRI systems, ranging from 125 to 130 dB(A), exceed this threshold [5]. Sound Reduction Strategies To address the sound issue in MRI, various solutions have been proposed. These include passive sound control methods, such as using earplugs, headphones, and sound-attenuating materials, as well as active sound control strategies that involve hardware modifications to the gradient coils [6].

©The Korean Magnetics Society. All rights reserved.

\*Corresponding author: Tel: +82-63-840-1236

Fax: +82-63-840-1082, e-mail: feel love83@hanmail.net

Additionally, there has been progress in software-based approaches that aim to optimize pulse sequences to reduce sound. However, hardware-based sound reduction methods often increase system complexity, introduce additional costs, and, in some cases, reduce the bore size and gradient performance. Therefore, leading MRI manufacturers have introduced low-noise imaging solutions such as GE's SilentScan, Siemens' QuietX, and Philips' ComforTone. These sequences are structurally similar to conventional MRI protocols but incorporate modified gradient waveforms characterized by smoother ramp-up and ramp-down profiles. This design significantly reduces acoustic noise, often bringing it within 10 dB(A) of ambient levels. However, the trade-off is an estimated 10% reduction in signal-to-noise ratio (SNR), primarily due to shortened data acquisition windows [7]. Recent efforts have focused on developing software technologies that mitigate these practical issues by minimizing highfrequency acoustic sound and reducing gradient strength, thus optimizing the gradient waveform. Research Objective Despite the development of software-based sound reduction techniques, detailed information about these methods is limited, and the effects of modifying gradient waveforms on image quality are not well understood [8, 9].

This study aims to quantitatively evaluate the changes in sound pressure levels (SPL) and image quality before and after the application of sound reduction techniques.



Fig. 1. (Color online) ACR Phantom.

The goal is to assess the clinical relevance and effectiveness of these sound reduction strategies, providing valuable criteria for reducing sound-related examination inaccuracies and patient discomfort while maintaining high image quality.

## 2. Materials and Methods

#### 2.1. Phantom study

A magnetic resonance accreditation phantom from the American College of Radiology (ACR) (model JM, Specialty Parts, San Diego, CA, USA) was utilized for the phantom measurement. The ACR phantom has an internal length of 148 mm and an internal diameter of 190 mm. It is filled with a solution containing 10 mM nickel

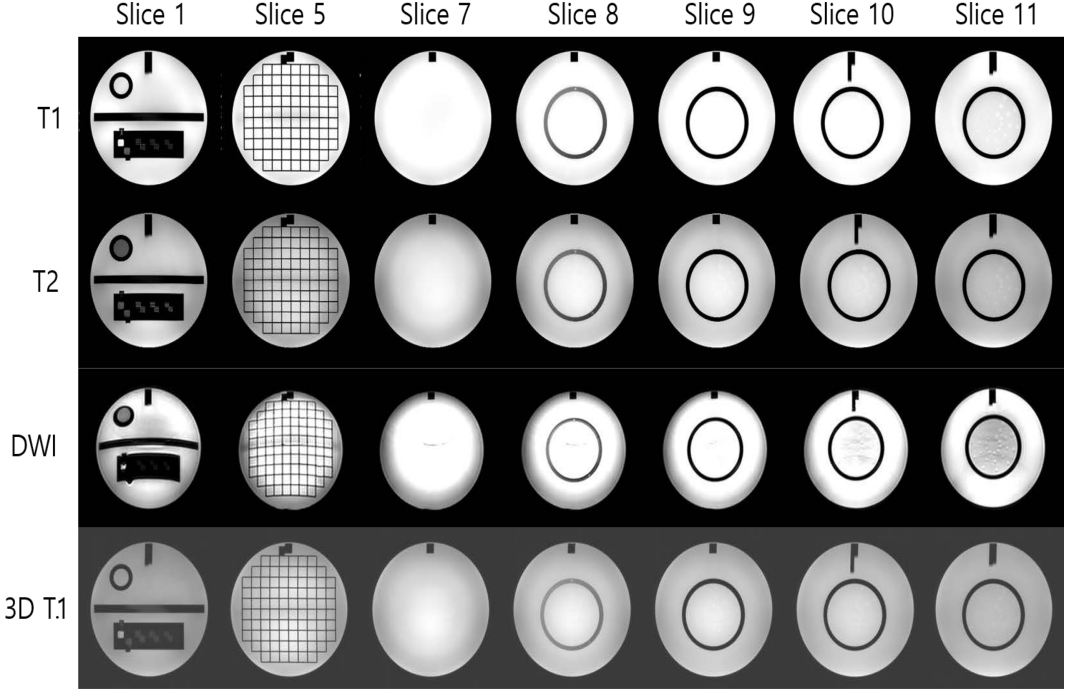


Fig. 2. T1, T2, DWI, and 3D T1 axial images were acquired without sound reduction and displayed at their respective default contrast levels and window settings.

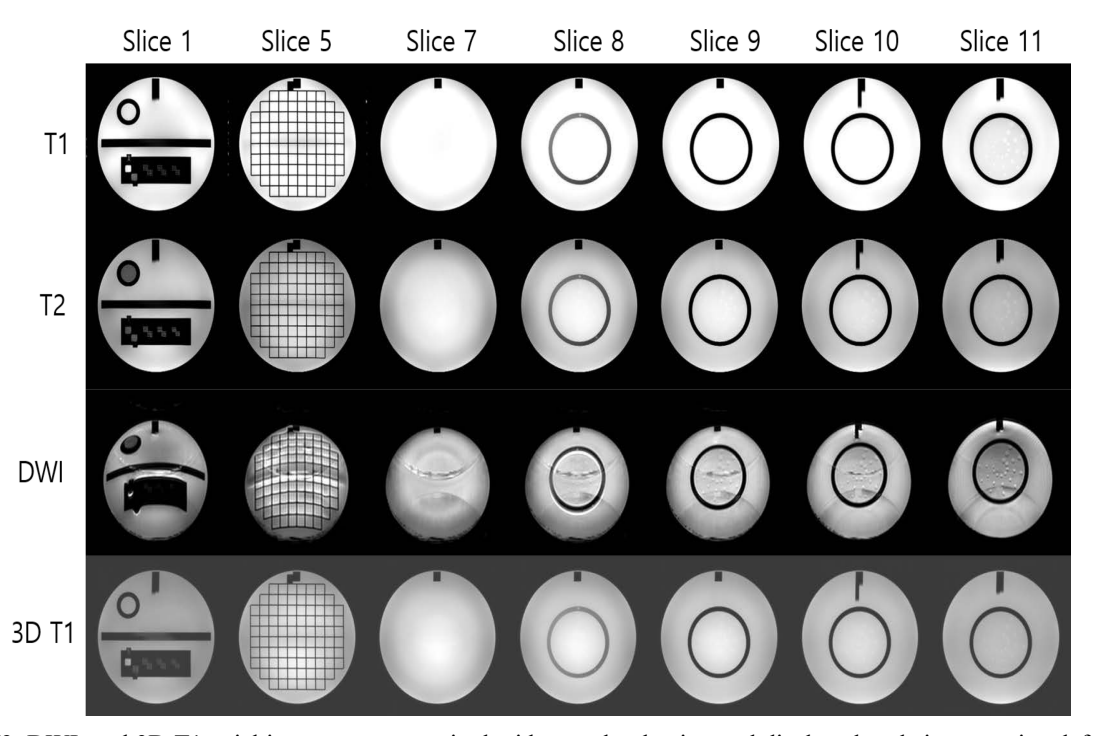


Fig. 3. T1, T2, DWI, and 3D T1 axial images were acquired with sound reduction and displayed at their respective default contrast levels and window settings.

chloride (NiCl2) and 75 mM sodium chloride (NaCl) [15]. The ACR phantom was precisely aligned and positioned at the center of each head coil in a specific spatial orientation, based on its nose and chin markers, and scanned at room temperature (21.0 °C) to prevent any temperature-related variations in the quantitative measurements (Fig. 1). This is a phantom study and no written informed consent was obtained.

## 2.2. MR equipment and protocol

The imaging equipment used in this study was a 3.0T MRI scanner (Ingenia, Philips Healthcare, The Netherlands), and a 32-channel head coil was employed as the receiving coil. The study methodology involved acquiring images both before and after the application of Sound reduction, a sound reduction technique provided by Philips. Standard images were obtained using an ACR phantom in accordance with quality control guidelines. The imaging sequences included axial T1-weighted, T2weighted, diffusion-weighted images (DWI) using an echo planar imaging (EPI) technique with strong gradient fields, and 3D gradient echo (GE) T1-weighted images, with each sequence repeated six times (Fig. 2 and 3). The 3D GE T1-weighted images were reconstructed into axial images with a slice thickness of 5 mm and a slice gap of 5 mm after the initial sagittal image acquisition. Detailed imaging parameters for each sequence are provided in

**Table 1.** Summary of Scan parameters.

Dawa at au	2D T1	2D T2	DWI	3D TFE*	
Parameter	$SE^*$	$FSE^*$	DWI	3D IFE	
TR (ms)	500	3000	2000	6.2	
TE (ms)	10	80	73	2.8	
Slice thickness (mm)	5	5	5	5	
Matrix	256*256	420*345	116*115	192*192	
Bandwidth (Hz/pixel)	102.0	68.1	0.5	45.5	
Scan time	2:12	1:08	0:25	1:43	

<sup>\*2</sup>D SE=2 Dimension Spin Echo, \*FSE=Fast Spin Echo, \*3D TFE=3 Dimension Turbo Field Echo

Table 1.

# 2.3. Image analysis

The acquired images were analyzed using Image J software (Version 1.47v, NIH, USA) to assess the following quality control parameters as specified by the ACR phantom guidelines: geometric accuracy, high-contrast spatial resolution, slice thickness accuracy, slice position accuracy, image intensity uniformity, percentage of ghosting artifacts, and low-contrast resolution. To demonstrate clinical relevance, the images were evaluated for compliance with the recommended acceptance criteria. Additionally, the reduction in sound pressure level (SPL) was compared by calculating the percentage difference, as

indicated by the SPL displayed on the equipment. Detailed descriptions of the measurement parameters based on the ACR MRI phantom guidelines are provided below.

## 2.3.1. Geometric accuracy

To evaluate the accuracy of lengths in the images compared to the actual dimensions of the object, the top-to-bottom, left-to-right, and diagonal distances were measured on ACR phantom image slices #1 and #5. For these measurements, all values were required to be within a 2 mm margin of error compared to the actual lengths.

## 2.3.2. High contrast spatial resolution

To evaluate the ability to distinguish small objects in the image, we visually evaluated the discernibility of closely positioned bright points. Slice #1 contains three groups of points arranged in the upper left and lower right quadrants. Each group consists of points with diameters of 1.1 mm, 1.0 mm, and 0.9 mm, decreasing in size from left to right. The evaluation involved determining whether these points could be distinctly resolved. In the upper left quadrant, the points were evaluated for left-right resolution, while in the lower right quadrant, they were assessed for up-down resolution, with four points needing to be distinguishable in each direction to be recorded as a measure of spatial resolution.

## 2.3.3. Slice thickness accuracy

To evaluate the accuracy of slice thickness, we measured the length of the bright signal ramp located in the center of the transverse bars on image slice #1. The evaluation was conducted using the following formula (Equation 1) to determine if the slices were accurately obtained at the specified thickness. All slice thicknesses must fall within a 0.7 mm margin of error around the target thickness of 5 mm.

# 2.3.4. Slice position accuracy

The difference in the left-right length of the pair of vertical bars located at the top of image slices #1 and #11 must be within 5 mm for both slices.

## 2.3.5. Image intensity uniformity

In the image of slice #7, a region of interest (ROI) with an area of 195-205 cm² was drawn in the homogeneous central region composed solely of water. The highest and lowest signal intensity areas within this ROI were identified. Signal intensity uniformity was then assessed using the following formula (Equation 2). The Percent Image Uniformity (PIU) value should be 82% or higher for systems operating at 3T or above.

#### 2.3.6. Ghost artifact

The presence of ghost artifacts is evaluated using slice #7 of the ACR MRI phantom image. The assessment involves measuring the signal intensity within a region of interest (ROI) located at the center of the image. Additionally, elliptical ROIs with a size of 10 cm are drawn outside the phantom, specifically on the top, bottom, left, and right sides. The signal intensities within these ROIs are measured and then substituted into the following formula (Equation 3) to calculate the percentage of ghost artifacts. The ghost signal percentage must be 0.025 or less.

## 2.3.7. Low contrast object detectability

The ability to distinguish low-contrast objects is evaluated using slices #8 through #11. Each slice contains 10 radially arranged spokes, with the size of the low-contrast objects decreasing as you move clockwise within a slice. Additionally, the contrast of the objects decreases progressively from slice #11 to slice #8. To meet the criteria, at least 37 out of the total 40 spokes must be distinguishable.

#### 2.4. Statistical analysis

The statistical analysis was conducted to determine whether there were significant differences in the data before and after the application of the Sound reduction technique. This analysis was performed using the paired samples t-test in SPSS version 21 (IBM Corp., Chicago, IL, USA). A p-value of less than 0.05 was considered indicative of a statistically significant difference.

## 3. Results

Geometric accuracy, excluding DWI, was within a 2 mm error range of the actual length according to ACR MRI phantom guidelines in all images, and the p-value was greater than 0.05, indicating no statistically significant difference in geometric accuracy before and after the application of the Sound reduction technique (Table 2). DWI images exhibited significant distortion regardless of Sound reduction application, precluding accurate measurements meaningless; The DWI images exhibited noticeable geometric distortions, localized signal dropouts, and artifacts related to magnetic susceptibility (Fig. 4). Particularly, mild signal loss and zig-zag distortion were identified in susceptibility-prone regions near the periphery of the phantom. These distortions were slightly more prominent after the application of the noise reduction technique. Therefore, DWI was excluded from further quality control evaluation.

Table 2. Geometric accuracy.

Sequence Sound reduction technique			ion technique	- n voluo
Sec	quence	without	with	p value
T1	#1 *RL	$190.36 \pm 0.11$	$190.21 \pm 0.12$	0.358
	#1 *AP	$190.61 \pm 0.13$	$190.19 \pm 0.12$	0.641
	#5 RL	$190.21 \pm 0.21$	$189.85 \pm 0.27$	0.176
	#5 AP	$189.81 \pm 0.15$	$190.23 \pm 0.05$	0.261
	#5 *RD	$189.93 \pm 0.21$	$190.15 \pm 0.19$	0.752
	#5 *LD	$190.12 \pm 0.17$	$189.75 \pm 0.08$	0.256
T2	#1 RL	$190.33\pm0.05$	$189.78 \pm 0.09$	0.425
	#1 AP	$190.21 \pm 0.11$	$189.81 \pm 0.12$	0.128
	#5 RL	$189.76\pm0.05$	$189.28\pm0.04$	0.525
	#5 AP	$190.12\pm0.06$	$189.56 \pm 0.12$	0.145
	#5 RD	$190.73 \pm 0.05$	$189.66 \pm 0.08$	0.235
	#5 LD	$189.68\pm0.14$	$189.43 \pm 0.21$	0.053
DWI	#1 RL	$182.85\pm0.95$	$178.11 \pm 0.61$	NA
	#1 AP	$184.15\pm0.41$	$183.56 \pm 0.35$	NA
	#5 RL	$185.52 \pm 0.57$	$184.19 \pm 0.47$	NA
	#5 AP	$183.61\pm0.35$	$175.71 \pm 0.39$	NA
	#5 RD	$184.60\pm0.52$	$181.42 \pm 0.51$	NA
	#5 LD	$185.71 \pm 0.13$	$183.45\pm0.42$	NA
3D	#1 RL	$190.16 \pm 0.11$	$189.51 \pm 0.23$	0.285
	#1 AP	$190.15 \pm 0.12$	$190.26 \pm 0.06$	0.625
	#5 RL	$189.82\pm0.17$	$191.08 \pm 0.21$	0.115
	#5 AP	$189.61 \pm 0.13$	$189.58 \pm 0.24$	0.486
	#5 RD	$191.17 \pm 0.25$	$190.78\pm0.16$	0.635
	#5 LD	$191.21 \pm 0.21$	$191.55 \pm 0.21$	0.490

RL=Right to Left, \*AP=Anterior to Posterior, \*RD=Right Diagonal, \*LD=Left Diagonal, Length values are presented as mean standard deviation. p-value was calculated using paired T-test, and p<0.05 is statistical significant. NA = Not applicable

High-contrast spatial resolution exceeded 1.0 mm, as per ACR MRI phantom guidelines, in all images, with no difference observed before and after Sound reduction application, resulting in no statistical value being reported (Table 3).

Table 3. High Contrast Spatial Resolution.

Sequence		Sound reduction technique		# volue
Sequ	ence	without	with	p value
T1	*UL	0.9	0.9	NA
11	*LR	0.9	0.9	NA
T2	UL	0.9	0.9	NA
	LR	0.9	0.9	NA
DWI	UL	NA	NA	NA
	LR	NA	NA	NA
3D	UL	1.0	1.0	NA
	LR	1.0	1.0	NA

<sup>\*</sup>UL=Upper to Left, \*LR=Lower to Right, NA=not applicable

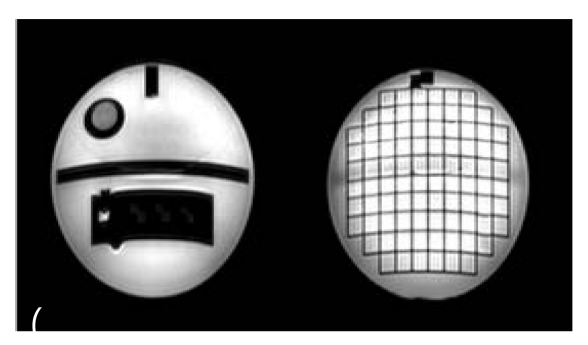
Slice thickness accuracy was within a 0.7 mm error range from the 5 mm guideline in all images, with p-values of 0.200 and 0.146 for T1 and 3D images, respectively, indicating no statistically significant difference in slice thickness accuracy before and after Sound reduction application. However, in T2 images, the p-value was less than 0.05, indicating a statistically significant difference (Table 4).

Slice position accuracy required that the measurements of slices #1 and #11 be within 5 mm (Table 5).

Image intensity uniformity was above 82.0% as per the ACR MRI phantom guidelines for 3.0T in all images except 3D. The p-values for T1, T2 images were greater than 0.05, indicating no statistically significant difference in intensity uniformity before and after Sound reduction

Table 4. Slice thickness accuracy.

Caguanaa	Sound reduction technique		n voluo
Sequence —	without	with	p value
T1	$4.96 \pm 0.07$	$4.92 \pm 0.02$	0.200
T2	$4.98 \pm 0.17$	$4.54 \pm 0.15$	< 0.05
DWI	NA	NA	NA
3D	$4.99 \pm 0.03$	$5.04 \pm 0.07$	0.146



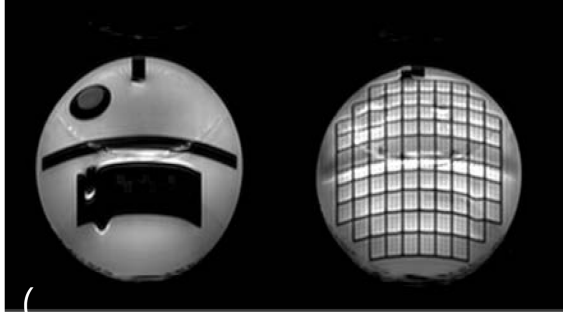


Fig. 4. DWI Slice 1, 5 axial images were displayed without sound reduction (A), and with sound reduction (B).

Table 5. Slice position accuracy.

Sequence —		Sound reduct	Sound reduction technique	
		without	with	p value
T1	#1	$-0.92 \pm 0.06$	$-0.68 \pm 0.07$	< 0.05
	#11	$-4.57 \pm 0.21$	$-4.63 \pm 0.11$	0.563
T2	#1	$\textbf{-0.93} \pm 0.07$	$-0.99 \pm 0.11$	0.045
	#11	$-4.31 \pm 0.25$	$\textbf{-4.69} \pm 0.28$	0.038
DWI	#1	NA	NA	NA
	#11	NA	NA	NA
3D	#1	$-1.83 \pm 0.21$	$-1.83 \pm 0.15$	0.929
	#11	$-4.48 \pm 0.11$	$-4.39 \pm 0.14$	< 0.05

application. However, as previously explained, the 3D images were evaluated based on reconstructed axial images, resulting in both images failing to meet the uniformity criteria (Table 6).

The ghost signal percentage was below 2.5%, as required by ACR MRI phantom guidelines, in all images. In T1, and 3D images, the p-value was less than 0.05, indicating a statistically significant difference in ghost signal percentage before and after Sound reduction application, whereas T2 had a p-value of 0.557, showing no statistically significant difference (Table 7).

Low-contrast detectability required a minimum of 37 discernible spokes from slices #8 to #11 according to ACR MRI phantom guidelines. All images met this criterion with a total of 40 discernible spokes, showing no difference before and after Sound reduction application; thus, no statistical p-value was reported (Table 8).

The sound pressure level reduction was converted into a percentage (%) before and after Sound reduction appli-

Table 6. Image intensity uniformity.

Sequence —	Sound reduction technique		n voluo
	without	with	p value
T1	$95.35 \pm 0.31$	$96.17 \pm 0.25$	0.145
T2	$87.51 \pm 0.35$	$86.52 \pm 0.46$	0.284
DWI	NA	NA	NA
3D	$81.36 \pm 0.23$	$82.41\pm0.17$	0.158

Table 7. Percent signal ghosting.

Caguanaa	Sound reducti	n voluo	
Sequence –	without	with	p value
T1	$0.0016 \pm 0.0004$	$0.0023 \pm 0.0005$	< 0.05
T2	$0.0017 \pm 0.0001$	$0.0015 \pm 0.0002$	0.528
DWI	NA	NA	NA
3D	$0.0008 \pm 0.0002$	$0.0011 {\pm}~0.0001$	< 0.05

Table 8. Low contrast object detectability.

Sequence		Sound reduction technique		p value
		without with		
T1	#8-#11	40	40	NA
T2	#8-#11	40	40	NA
DWI	#8-#11	40	40	NA
3D	#8-#11	40	40	NA

**Table 9.** Sound pressure level.

	Sound reduction technique			
Sequence	without	with	Reduction	
	(dB(A))	(dB(A))	(%)	
T1	-1.5	-1.1	27.3%	
T2	10.5	5.3	49.6%	
DWI	25	6.0	72.5%	
3D	17.3	5.2	70.1%	

cation, showing a reduction of 15% in T1, approximately 40% in T2 and approximately 70% in DWI and 3D (Table 9).

#### 4. Discussion

MR is extensively utilized for the precise diagnosis of diseases and biomedical research by leveraging signals emitted from hydrogen nuclei within the human body under the influence of a magnetic field [10]. However, sound generation is an inevitable byproduct of the magnetic field generation process, prompting the development of numerous methods to address this issue over the past several decades. As a result, various studies have been conducted to reduce sound during MRI examinations.

JP McNulty et al. explored passive sound control methods, such as earplugs, headphones, and sound-damping materials, which are among the most basic strategies for sound reduction. However, they found that the effectiveness of these methods diminished as the magnetic field strength increased, and they were unable to reduce the sound below a specific sound pressure level 60 dB(A) [11].

In addition to the use of hearing protection, hardware-based active sound control has also progressed. This approach aims to minimize vibrations in other parts of the system by placing the gradient coils in a vacuum chamber to block the transmission of vibrations through the air, supporting the gradient coils independently to block solid vibrations, and reducing eddy currents induced by RF coils and shielding [12, 13]. Yaohui Wang et al. designed an asymmetric gradient coil system to evaluate sound

reduction, but they did not compare the impact on image quality, which differentiates their study from the present one. Furthermore, this approach primarily focuses on shielding existing sound or on the structural system of the equipment itself, making it challenging to implement practically [14].

To address these limitations, various software-based sound reduction technologies have emerged. These methods are proprietary to the equipment manufacturers, making it difficult to compare the underlying principles due to the lack of detailed disclosures. However, these techniques generally reduce sound by decreasing or optimizing the slew rate, which refers to the rise and fall time of the gradients [15]. During this process, the gradient coils operate at near-stable levels with very small incremental changes, resulting in minimal additional sound during MRI scans [16]. Due to these advantages, several studies have focused on software-based sound reduction technologies.

Eric Y. Pierrel et al. compared the signal-to-sound ratio (SNR) and radiologists' qualitative evaluations of image quality before and after applying Siemens' QuietX, one of the sound reduction techniques, but their study was limited to the fast spin echo (FSE) sequence. In contrast, the present study includes a comparison of various techniques, such as inversion recovery (IR), echo planar imaging (EPI), and 3D gradient echo (GE), in addition to FSE [17].

M. Wyss et al. compared sound pressure levels and image quality using two sound reduction techniques from Philips, Softone and Sound reduction. The earlier Softone technique allowed for a selectable reduction level between 1 and 5 but could not be applied when the gradient mode was at maximum. The more recent Sound reduction, developed to address these limitations, automatically reduces sound pressure levels to below 98 dB(A), with up to an 80% sound reduction, without restricting the gradient mode [18]. Yamashiro et al. also compared sound pressure levels and image quality before and after applying the Sound reduction technique [7]. However, both studies primarily focused on SNR as the sole measure of image quality, whereas the current study conducts a more comprehensive quantitative analysis using ACR phantom images, following MRI quality control guidelines, thereby offering a broader evaluation.

The results of this study showed no statistically significant difference in most images before and after the application of Sound reduction, except for the significantly distorted diffusion-weighted imaging (DWI). However, during the application of Sound reduction, the alteration of the gradient waveform and reduction in the slew rate

resulted in statistically significant differences in some parameters. including slight prolongation of TE, reduced sampling efficiency, and a moderate decline in SNR. Nonetheless, quantitative analysis confirmed that all images met the MRI ACR phantom quality control guidelines. This indicates that even with the use of the Sound reduction technique within diagnostic limits according to ACR criteria image quality can be obtained.

This study has some limitations, including the fact that it did not involve human subjects, and the significant distortion in DWI made the geometric accuracy measurements meaningless, regardless of whether Sound reduction was applied, leading to the exclusion of DWI from further quantitative analysis. Additionally, the evaluation of 3D GE T1 images reconstructed into axial slices resulted in both images failing to meet the uniformity guidelines. Therefore, further studies are needed to address these limitations. However, unlike previous studies, this research provides a quantitative analysis of the effectiveness of sound reduction technologies across various imaging techniques by evaluating ACR phantom images according to quality control criteria, thereby laying a foundation for future research.

## 5. Conclusion

In conclusion, the application of the Sound reduction technique during MRI examinations can significantly reduce sound, thereby alleviating patient discomfort and improving the accuracy of the examination, while still providing image quality within diagnostic limits according to ACR criteria compared to standard imaging.

## **Acknowledgments**

This research was supported by Wonkwang Health Science University.

## References

- [1] J. H. Yoon, J. S. Kim, and H. R. Lee, Korean J. Otorhinolaryngol. Head. Neck. Surg. 46, 1023 (2003).
- [2] M. E. Ravicz, J. R. Melcher, and N. Y.-S. Kiang, J. Acoust. Soc. Am. 108, 1683 (2000).
- [3] Y. Hattori, H. Fukatsu, and T. Ishigaki, Nagoya J. Med. Sci. **69**, 23 (2007).
- [4] D. Tomasi, E. C. Caparelli, L. Chang, and T. Ernst, Neuroimage **27**, 377 (2005).
- [5] A. Sheppard, Y. C. Chen, and R. Salvi, The Hearing Journal, **71**, 30 (2018).
- [6] B. W. Rudd, T. C. Lim, J.-H. Lee, and M. Li, Noise Control Engineering Journal, **61**, 41 (2013).

- [7] T. Yamashiro, K. Morita, and K. Nakajima, Magn. Reson. Imaging, **63**, 170 (2019).
- [8] B. Heismann, M. Ott, and D. Grodzki, Magn. Reson. Med. 73, 1104 (2015).
- [9] A. Katsunuma, H. Takamori, Y. Sakakura, Y. Hamamura, Y. Ogo, and R. Katayama, Magn. Reson. Mater. Phys. Biol. Med. 13, 139 (2002).
- [10] D. Pradeep, M. K. Tembhre, A. S. Parihar, and C. Rao, Biomedical Imaging Instrumentation, Academic Press, Newyork (2022) pp. 45-66.
- [11] J. P. McNulty and S. McNulty, Radiography **15**, 320 (2009).
- [12] A. M. Goldman, W. E. Gossman, and P. C. Friedlander, Radiology 173, 549 (1989).
- [13] M. McJury, R. W. Stewart, D. Crawford, and E. Toma, Magn. Reson. Imaging 15, 319 (1997).

- [14] Y. Wang, F. Liu, E. Weber, F. Tang, J. Jin, Y. Tesiram, and S. Crozier, Concepts Magn. Reson. Part B: Magn. Reson. Eng. 45, 85 (2015).
- [15] W. A. Edelstein, R. A. Hedeen, R. P. Mallozzi, S. A. El-Hamamsy, R. A. Ackermann, and T. J. Havens, Magn. Reson. Imaging 20, 155 (2002).
- [16] S. Alibek, M. Vogel, W. Sun, D. Winkler, C. A. Baker, M. Burke, and H. Gloger, Diagn. Interv. Radiol. 20, 360 (2014).
- [17] E. Y. Pierre, D. Grodzki, G. Aandal, B. Heismann, C. Badve, V. Gulani, J. L. Sunshine, M. Schluchter, K. Liu, and M. A. Griswold, Invest. Radiol. 49, 620 (2014).
- [18] M. Wyss, I. Dobrev, J. H. Sim, T. D. J. Sartoretti, A. Najafi, M. Koepfli, A. M. Huber, and C. A. Binkert, Proceedings of the Conference ECR 2018, C-2186 (2018).